The Antiproton Signal of the Galactic Supersymmetric Dark Matter

Neutrino Telescopes - Venezia - February 25 1999

P. Salati, Laboratoire LAPTH and Université de Savoie

1) Antiproton production in our galaxy

2) BESS 95 & supersymmetric antiprotons
Bottino, Donato, Fornengo & Salati PR D58 (1998) 123503

3) Primary vs secondary antideutons
Donato, Fornengo & Salati

4) The instruments : balloon vs space

5) Discussion & future prospects

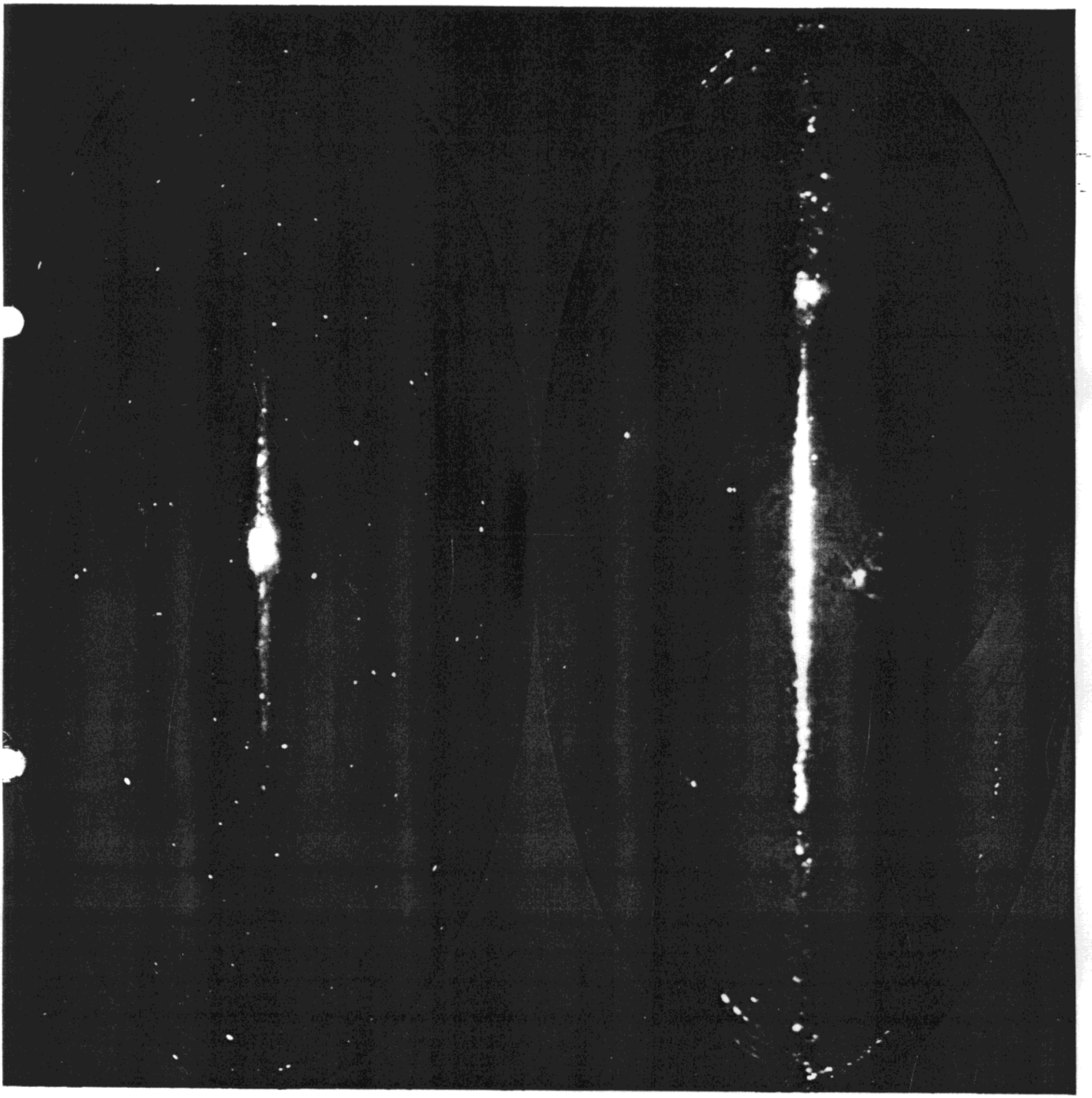

Antiproton production in our galaxy

Diffusion process :

$$\frac{\partial n}{\partial t} = 0 = K\Delta n + 2h\delta(z)q - 2h\delta(z)\Gamma n$$

Steady state

$pH \longrightarrow \bar{p} \ldots$

$$\bar{p}\ \text{source} = q = 4\pi n_H \int \frac{d\sigma}{dE_{\bar{p}}} \phi_p \, dE_p$$

Spallation $\Gamma = \sigma n_H v$

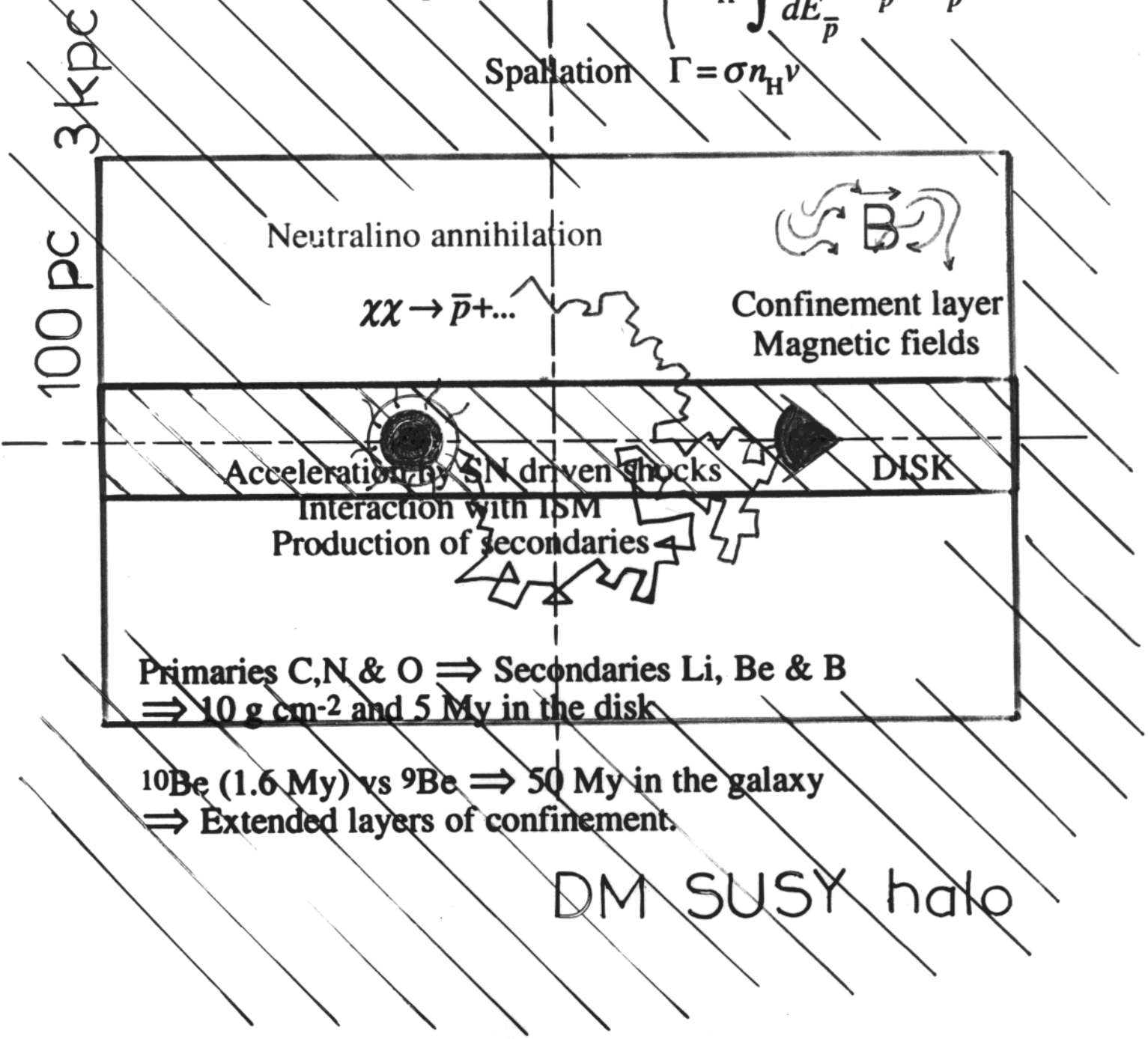

Primaries C,N & O $\Rightarrow$ Secondaries Li, Be & B
$\Rightarrow$ 10 g cm^{-2} and 5 My in the disk

^{10}Be (1.6 My) vs ^{9}Be $\Rightarrow$ 50 My in the galaxy
$\Rightarrow$ Extended layers of confinement.

DM SUSY halo

$$K_o = 6 \times 10^{27} \text{ cm}^2 \text{ s}^{-1}$$

$$K = K_o \left\{ 1 + R \right\}^{0.6}$$

Ficenec et al

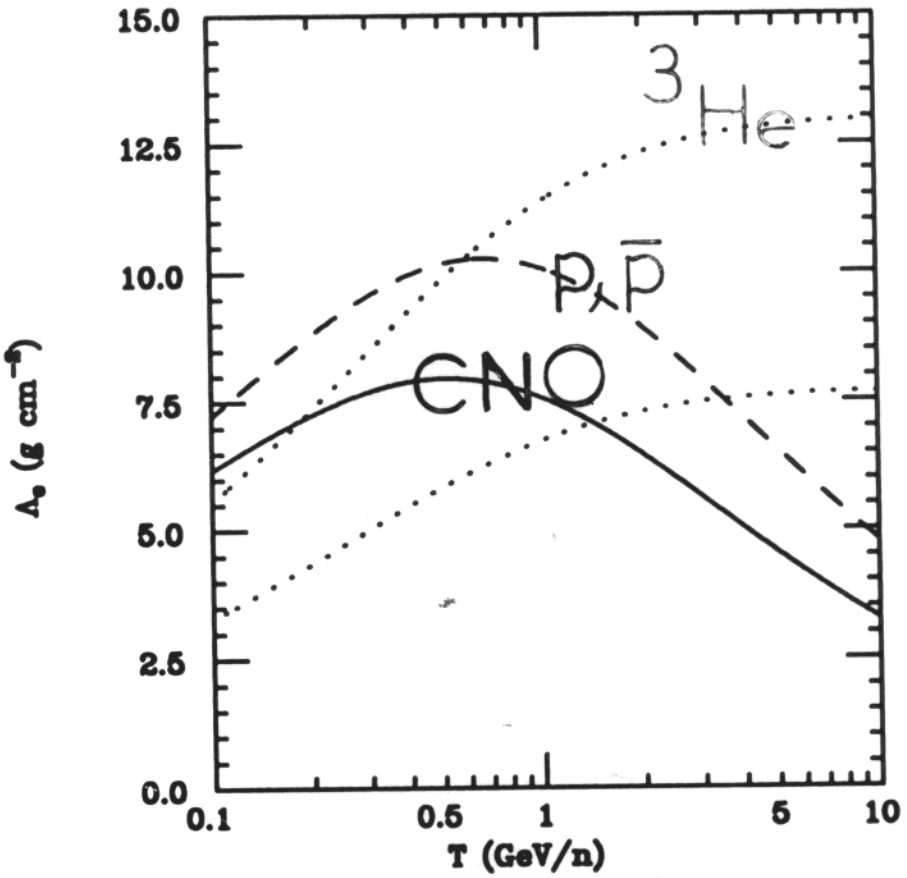

Figure 4

$$\chi^2_{red} = 0.83$$

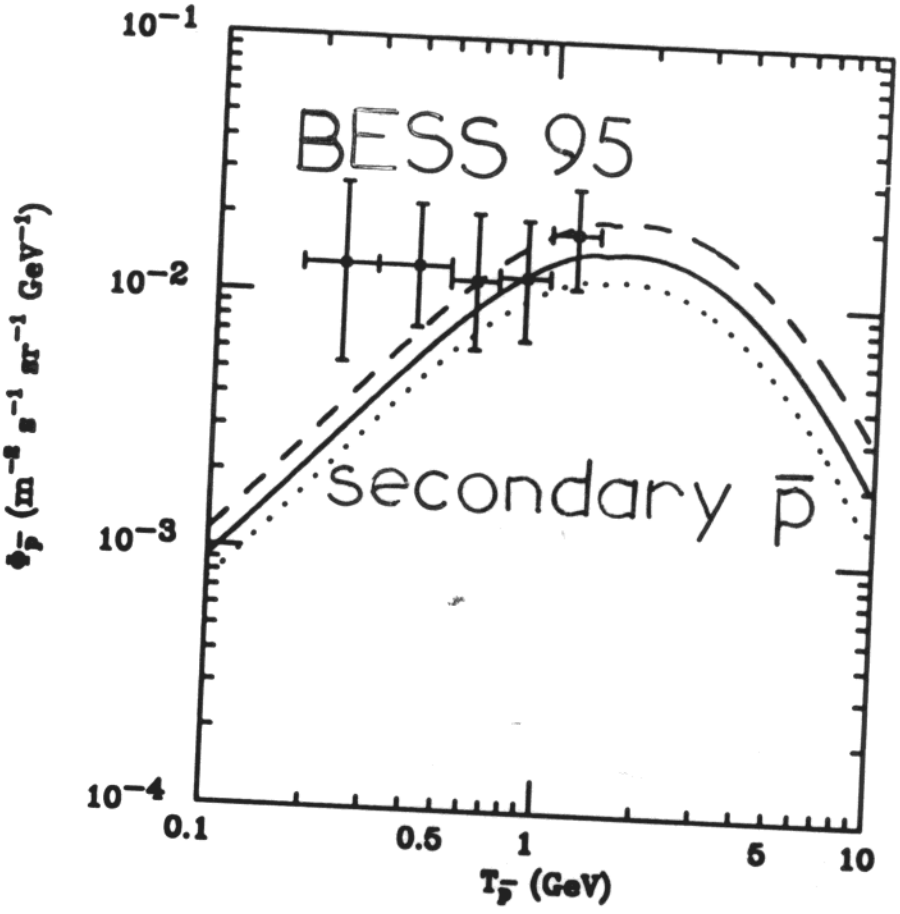

Figure 1

SUSY analysis

a. $\chi^2_{red} < 2.2$

b. $0.03 < \Omega_\chi h^2 < 0.7$

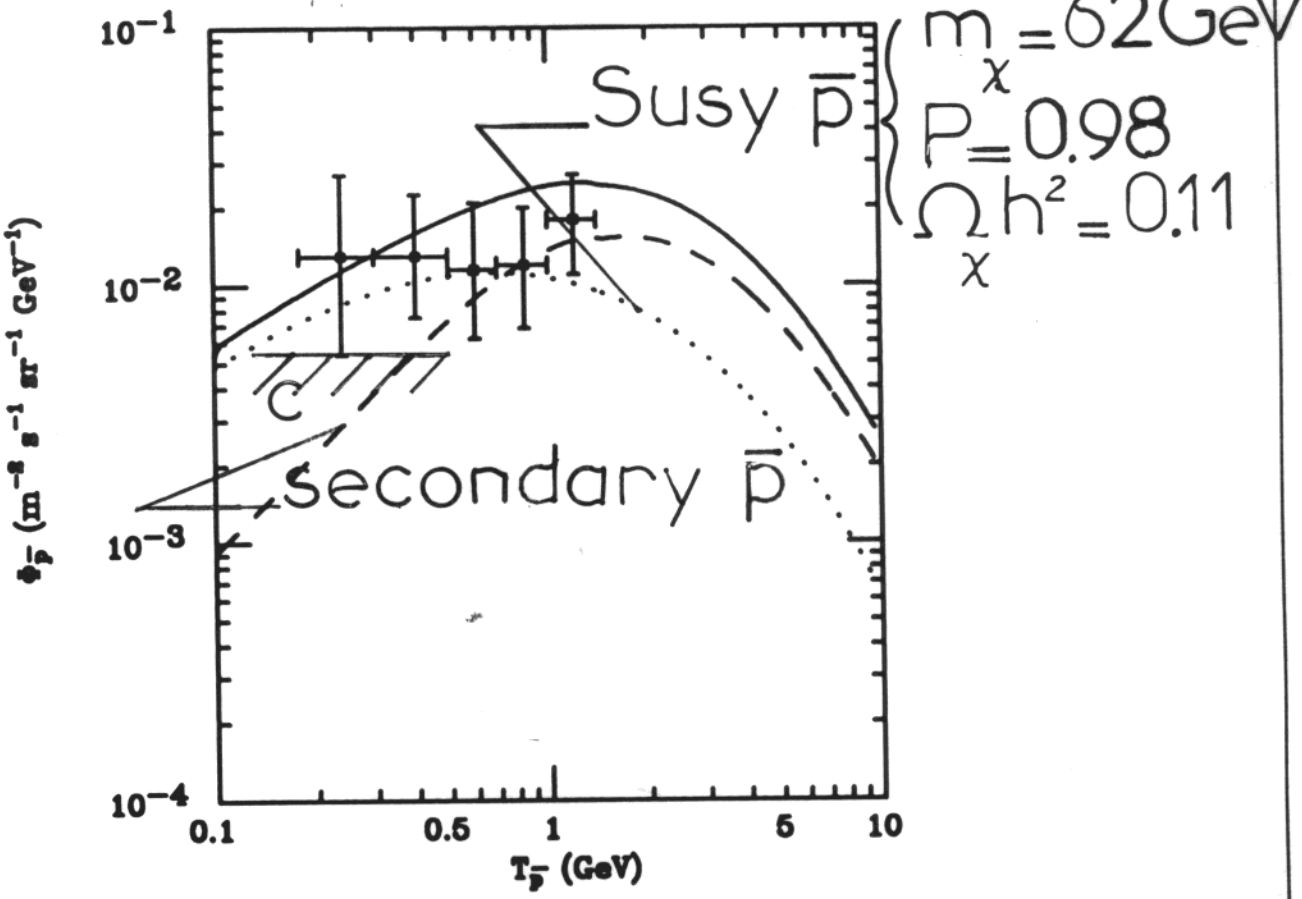

Figure 10

Compatible with
BESS

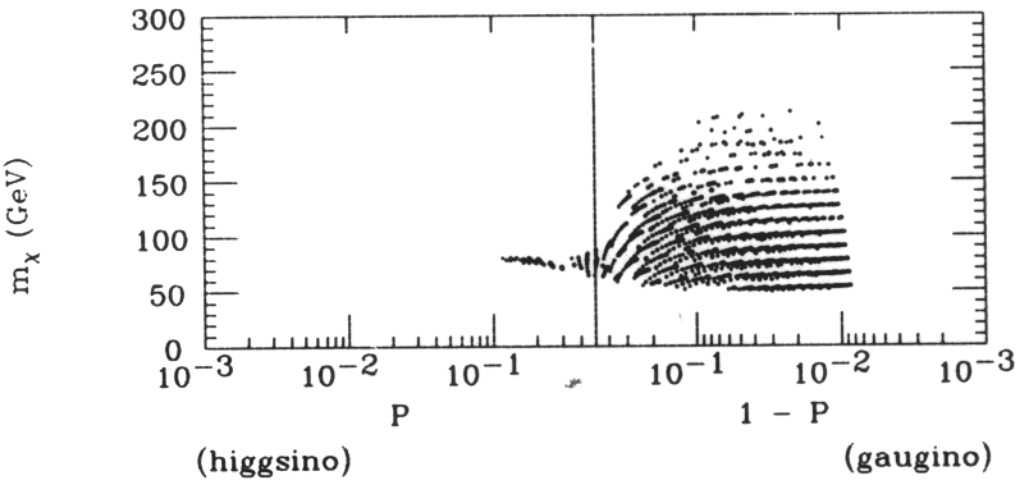

Figure 12 (b)

$\chi^2_{red} > 4$

Excluded

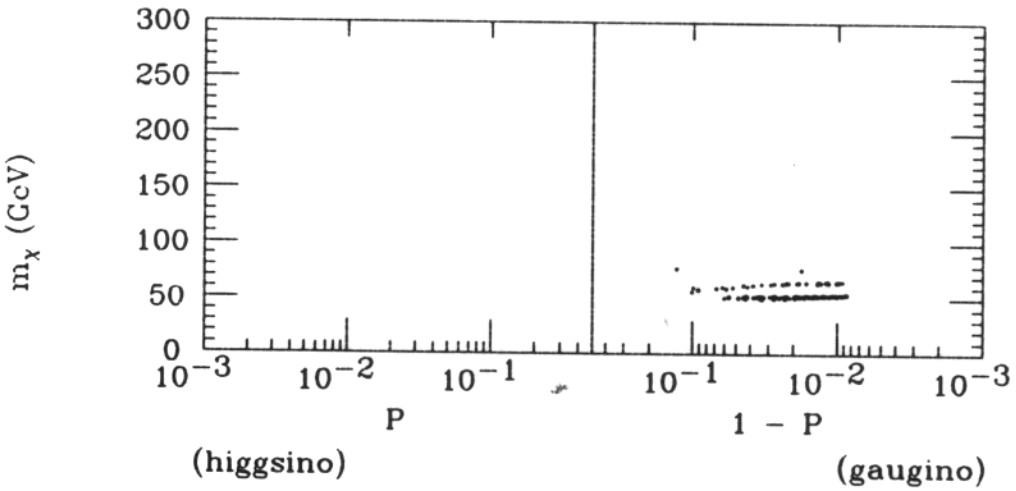

Figure 13 (b)

Excluded Configurations

$$\chi^2_{\text{red}} \geq 4$$

Flattened Galactic Halo with $f = 0.5$

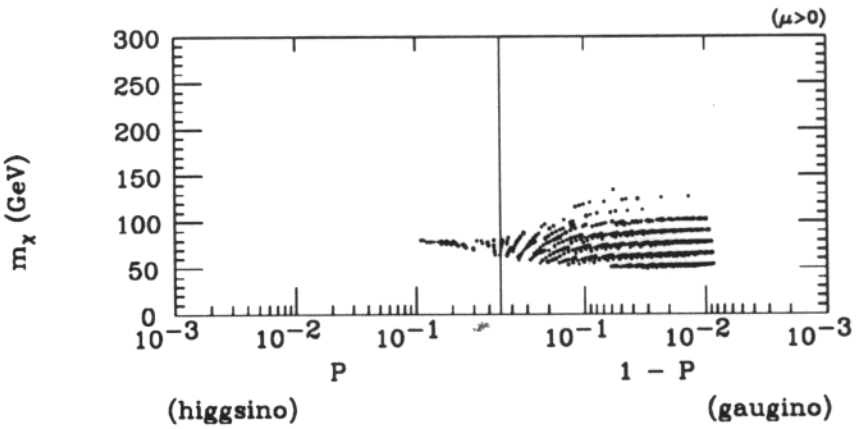

Figure 14 (b)

Figure 1: Scatter plot in the P–m_χ plane for the configurations excluded by the BESS 95 data when the galactic halo is flattened by a factor of $f = 0.5$.

Excluded Configurations

$$\chi^2_{\rm red} \geq 4$$

Flattened Galactic Halo with $f = 0.5$

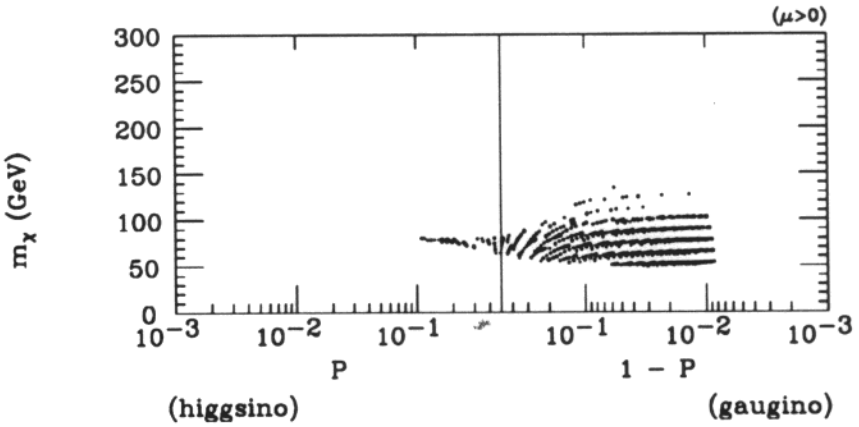

Figure 14 (b)

Figure 1: Scatter plot in the P–m_χ plane for the configurations excluded by the BESS 95 data when the galactic halo is flattened by a factor of $f = 0.5$.

Antiprotons & Direct Detection

$$\rho_l = 0.4 \text{ GeV cm}^{-3}$$

$$\chi^2_{\text{red}} \leq 2.2 \qquad 0.03 \leq \Omega h^2 \leq 0.7 \qquad \textbf{c)}$$

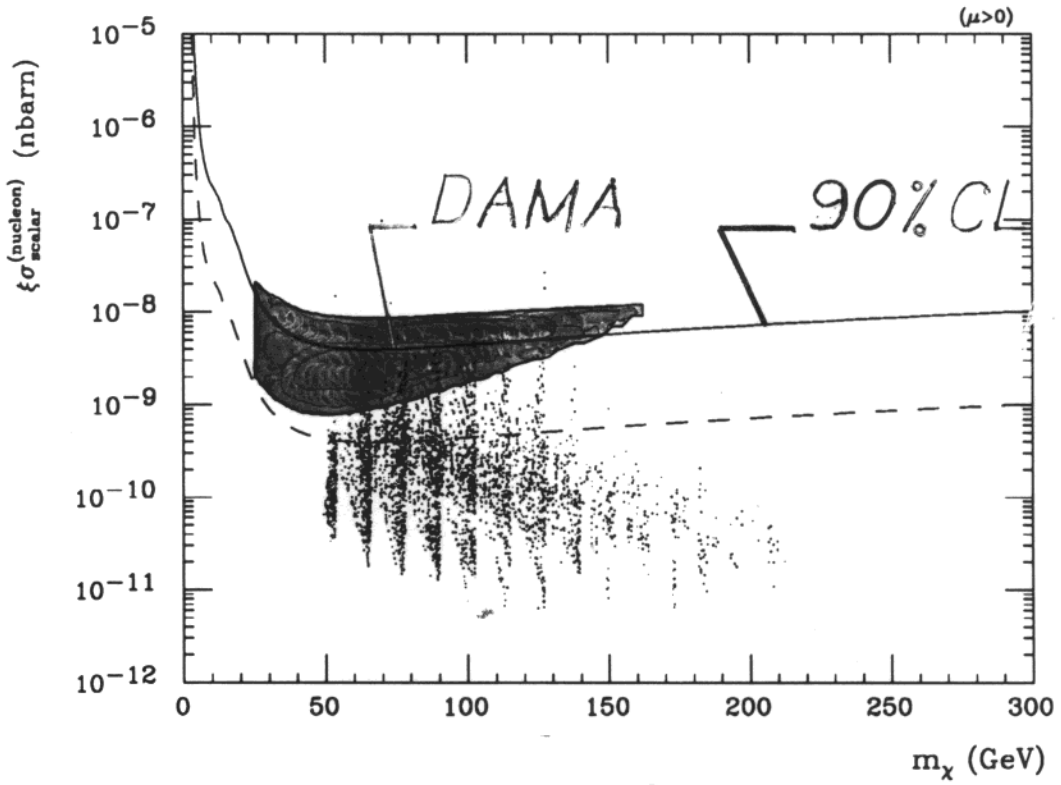

Figure 15 (b)

Figure 2: Scatter plot of the values of $\xi\sigma^{\text{nucleon}}_{\text{scalar}}$ versus the neutralino mass for the configurations compatible with BESS 95. The region delimited by a closed contour is the one singled out by the DAMA experiment as possibly indicative of an annual modulation effect.

Antideuterium Production in p-p Collisions & Neutralino Annihilations

$$d\mathcal{N}_X = \mathcal{F}_X(\sqrt{s}, \vec{k_X})\, d^3\vec{k_X} = \frac{1}{\sigma_{tot}} d^3\sigma_X(\sqrt{s}, \vec{k_X})$$

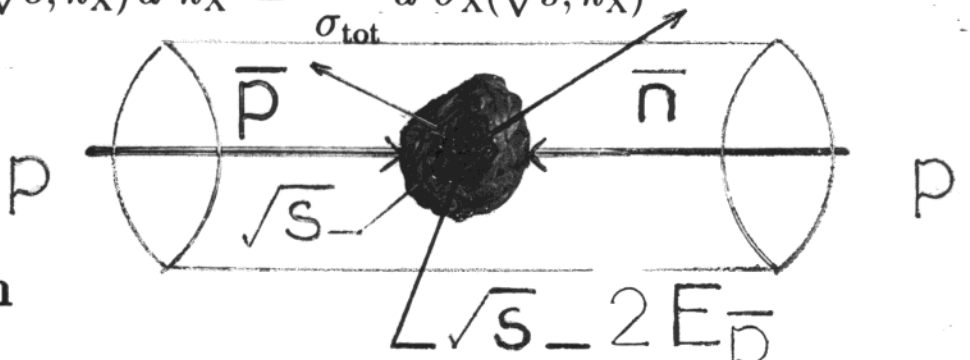

1) Factorization

$$\mathcal{F}_{\bar{p},\bar{n}}(\sqrt{s}, \vec{k_{\bar{p}}}, \vec{k_{\bar{n}}}) = \frac{1}{2}\mathcal{F}_{\bar{p}}(\sqrt{s}, \vec{k_{\bar{p}}})\, \mathcal{F}_{\bar{n}}(\sqrt{s} - 2E_{\bar{p}}, \vec{k_{\bar{n}}}) + \left(\vec{k_{\bar{p}}} \leftrightarrow \vec{k_{\bar{n}}}\right)$$

2) Coalescence

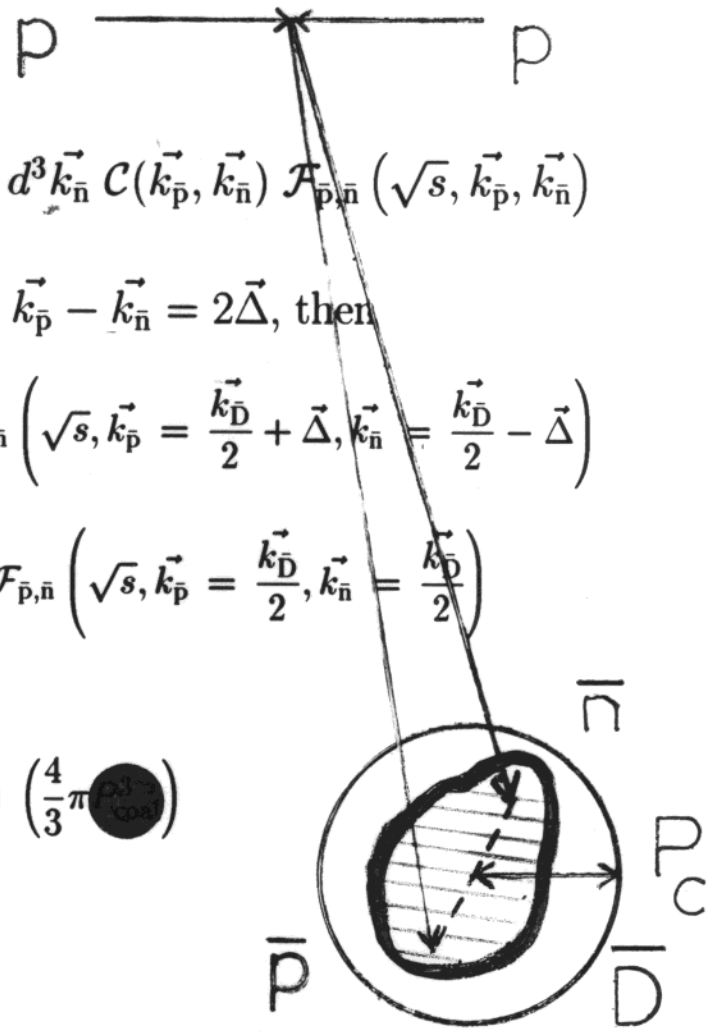

$$\mathcal{F}_{\bar{D}}(\sqrt{s}, \vec{k_{\bar{D}}})\, d^3\vec{k_{\bar{D}}} = \int d^3\vec{k_{\bar{p}}}\, d^3\vec{k_{\bar{n}}}\, C(\vec{k_{\bar{p}}}, \vec{k_{\bar{n}}})\, \mathcal{F}_{\bar{p},\bar{n}}\left(\sqrt{s}, \vec{k_{\bar{p}}}, \vec{k_{\bar{n}}}\right)$$

Because $\vec{k_{\bar{p}}} + \vec{k_{\bar{n}}} = \vec{k_{\bar{D}}}$ and $\vec{k_{\bar{p}}} - \vec{k_{\bar{n}}} = 2\vec{\Delta}$, then

$$\mathcal{F}_{\bar{D}}(\sqrt{s}, \vec{k_{\bar{D}}}) = \int d^3\vec{\Delta}\, C(\vec{\Delta})\, \mathcal{F}_{\bar{p},\bar{n}}\left(\sqrt{s}, \vec{k_{\bar{p}}} = \frac{\vec{k_{\bar{D}}}}{2} + \vec{\Delta}, \vec{k_{\bar{n}}} = \frac{\vec{k_{\bar{D}}}}{2} - \vec{\Delta}\right)$$

$$\mathcal{F}_{\bar{D}}(\sqrt{s}, \vec{k_{\bar{D}}}) \simeq \left\{\int d^3\vec{\Delta}\, C(\vec{\Delta})\right\} \mathcal{F}_{\bar{p},\bar{n}}\left(\sqrt{s}, \vec{k_{\bar{p}}} = \frac{\vec{k_{\bar{D}}}}{2}, \vec{k_{\bar{n}}} = \frac{\vec{k_{\bar{D}}}}{2}\right)$$

with

$$\int \frac{E_{\bar{D}}}{E_{\bar{p}}\, E_{\bar{n}}} d^3\vec{\Delta}\, C(\vec{\Delta}) \simeq \left(\frac{m_{\bar{D}}}{m_{\bar{p}}\, m_{\bar{n}}}\right)\left(\frac{4}{3}\pi P_{coal}^3\right)$$

• p-p collisions

$$p + p \rightarrow \bar{p} \text{ or } \bar{D}$$

$$E_{\bar{D}} \frac{d^3\sigma_{\bar{D}}}{d^3\vec{k}_{\bar{D}}} = \left(\frac{m_{\bar{D}}}{m_{\bar{p}}\, m_{\bar{n}}}\right) \left(\frac{4}{3}\pi \; \text{[redacted]}\right) \times \frac{1}{2\sigma_{tot}} \times$$

$$\times \left\{ E_{\bar{p}} \frac{d^3\sigma_{\bar{p}}}{d^3\vec{k}_{\bar{p}}} \left(\sqrt{s}, \vec{k}_{\bar{p}}\right) \; E_{\bar{n}} \frac{d^3\sigma_{\bar{n}}}{d^3\vec{k}_{\bar{n}}} \left(\sqrt{s} - 2E_{\bar{p}}, \vec{k}_{\bar{n}}\right) + \left(\vec{k}_{\bar{p}} \leftrightarrow \vec{k}_{\bar{n}}\right) \right\}$$

• Neutralino Annihilations

$$\chi + \chi \rightarrow \bar{p} \text{ or } \bar{D}$$

$$\sqrt{s} = 2\, m_{\chi}$$

and

$$\frac{dN_{\bar{D}}}{dE_{\bar{D}}} = \left(\frac{4 \; \text{[redacted]}}{3\, k_{\bar{D}}}\right) \left(\frac{m_{\bar{D}}}{m_{\bar{p}}\, m_{\bar{n}}}\right) \times \sum_h B_{\chi h} \left\{ \frac{dN^h_{\bar{p}}}{dE_{\bar{p}}} (E_{\bar{p}} = E_{\bar{D}}/2) \right\}^2$$

whereas

$$\frac{dN_{\bar{p}}}{dE_{\bar{p}}} = \sum_h B_{\chi h} \frac{dN^h_{\bar{p}}}{dE_{\bar{p}}}$$

$$q_X^{\text{susy}} = \langle \sigma v \rangle \; \frac{dN_X}{dE_X} \; \left\{ \frac{\rho_\chi}{m_\chi} \right\}^2$$

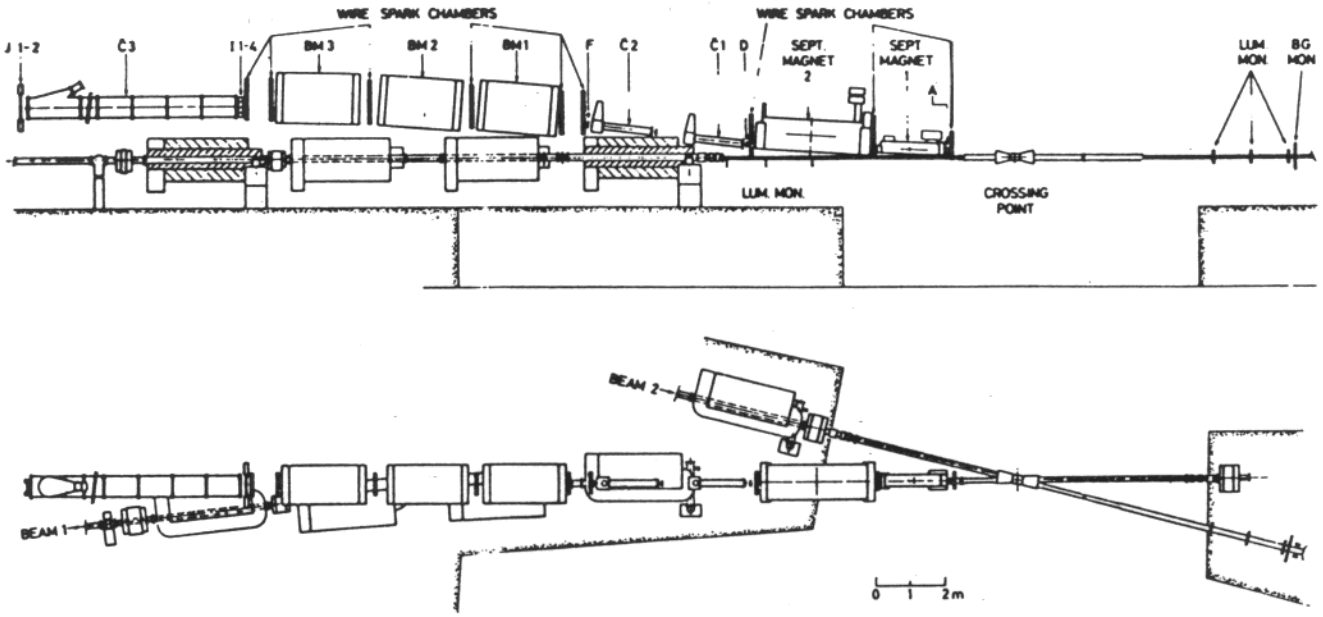

Fig. 1. Side and top views of the small angle spectrometer (SAS), located above the ISR beam 1. BM 1,2,3 are bending magnets, LUM MON is a set of counters for measuring the ISR luminosity. BG MON is a set of counters used to distinguish beam/beam from beam/gas events (see text).

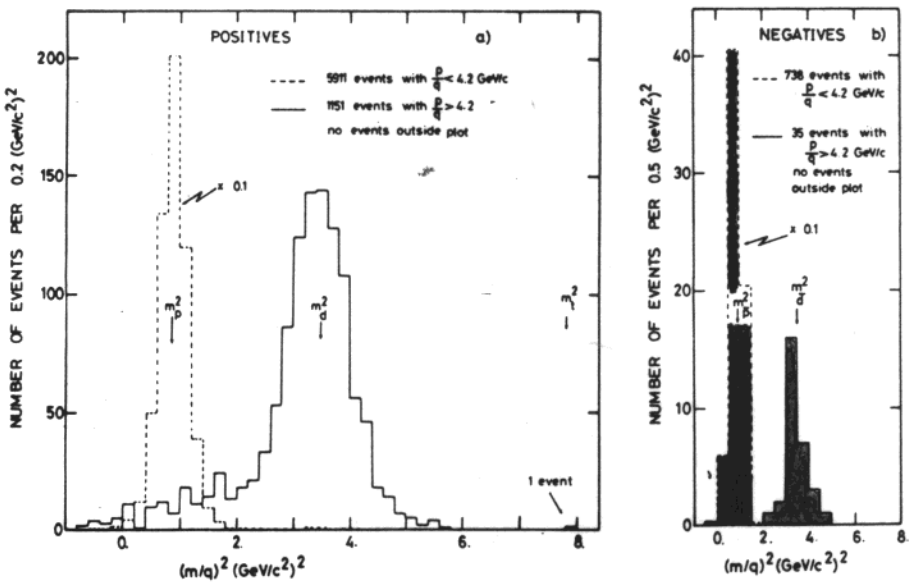

Fig. 3. (a) Distribution of $(m/q)^2$ for positive particles with $(p/q) < 4.2$ GeV/c (dashed lines) and $(p/q) >$ GeV/c (full lines). m is the particle mass and q its charge per electron charge. (b) Same as (a) for negative particles.

ISR 1975

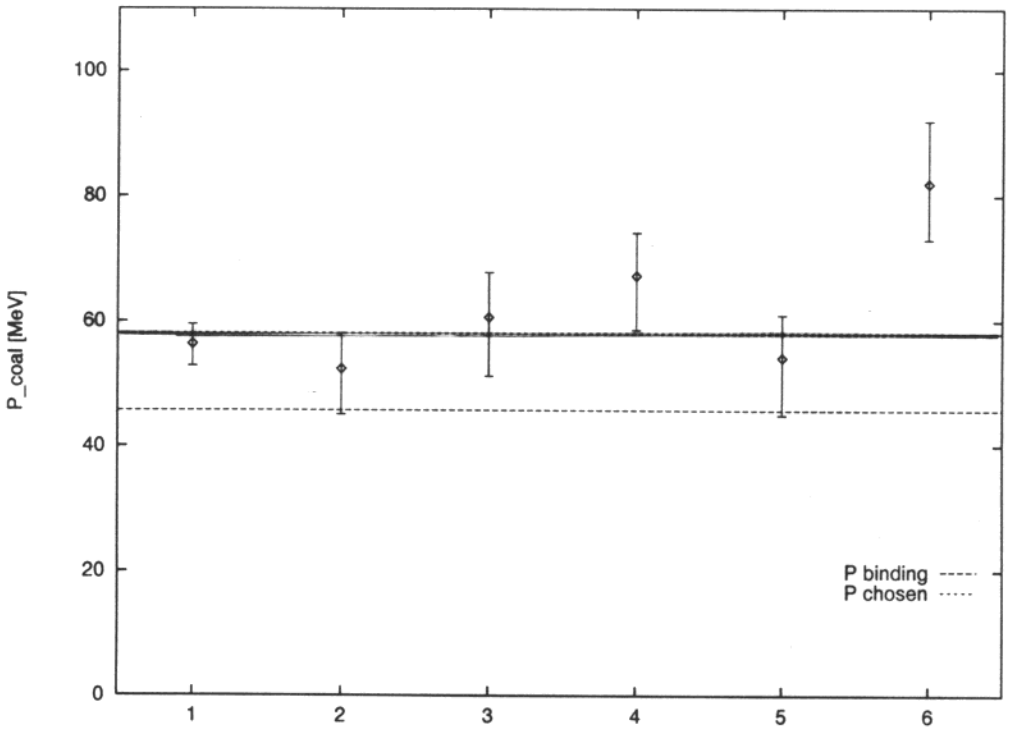

Figure 1: This figure displays various experimental constraints on the coalescence momentum P_{coal}, the only free parameter of the model discussed in section (2). Points 1 and 2 are from Serpukhov with $\sqrt{s}$= 11.5 GeV while all the other data have been collected at the ISR at $\sqrt{s}$ = 53 GeV. A coalescence momentum P_{coal} of order 60 MeV provides a reasonable fit of all the points but the last one.

$$pp \longrightarrow \overline{D}\, X$$

Valeurs de $E\frac{d^3\sigma}{dp^3}\Big|_{\overline{D}}$

#	p_L	p_T	µb/GeV^2
1	0	1.14	$(9.1\pm1.6)\times10^{-5}$
2	0	1.50	$(2.2\pm0.8)\times10^{-5}$
3	4.8	0.16	$(6.8\pm2.7)\times10^{-2}$
4	5.56	0.21	$(5.6\pm1.9)\times10^{-2}$
5	6.62	0.30	$(1.4\pm0.6)\times10^{-2}$

Susy & Secondary Antideuterium Flux

$m_\chi = 60.4$ GeV

$P = 0.84$: mostly gaugino

$\Omega_\chi h^2 = 0.02$

Donato, Fornengo & Salati, preliminary

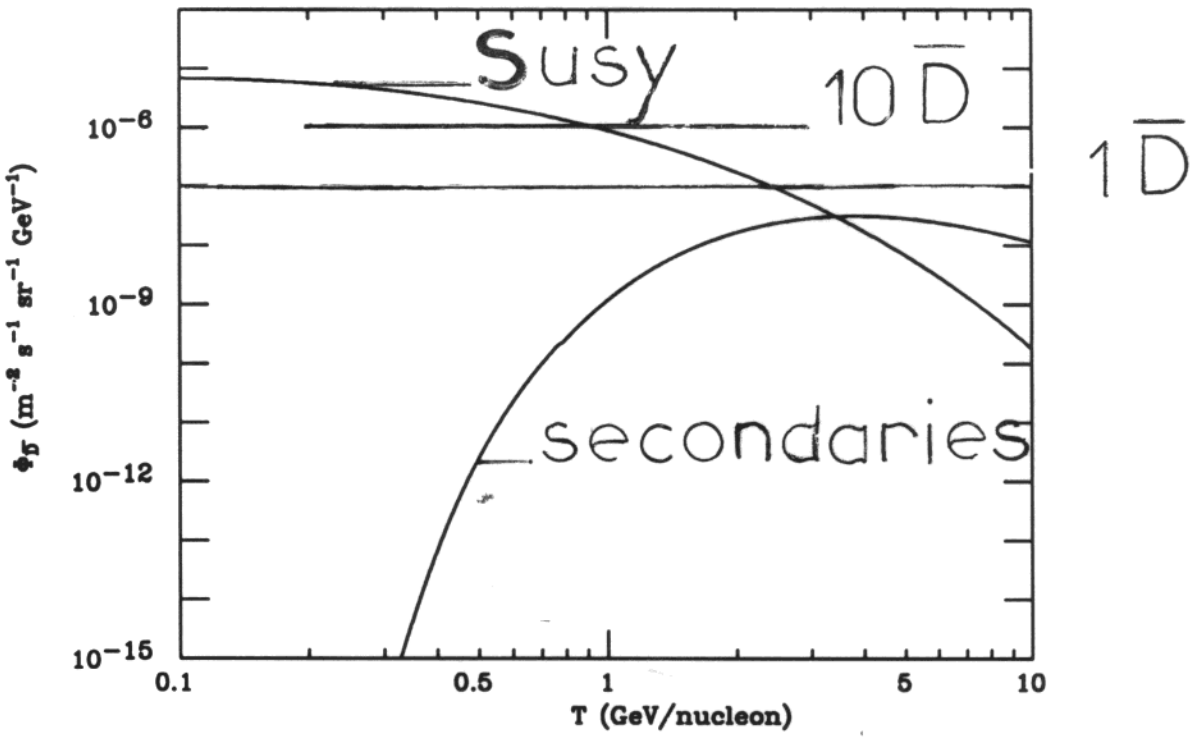

Figure 9: The IS antideuton flux is presented as a function of the kinetic energy per nucleon. The primary SUSY flux emerges at low energy while the secondary antideutons are most visible at energies in excess of a few GeV/n.

The instruments

- Balloon-borne experiments.

IMAX : 16 antiprotons accumulated with an acceptance of $\Omega ST = 260\ m^2\ sr\ s$

BESS 95 : 43 low-energy antiprotons with an acceptance of $\Omega ST = 2\times10^3\ m^2\ sr\ s$

Stratosphere $\Rightarrow$ 5 g cm^{-2} of air

Geomagnetic suppression factor

$$\left.\frac{pc}{Ze}\right|_{min} = \frac{\mu}{R^2}\frac{\cos^4 L}{\left[1+\sqrt{1+\cos\theta\cos^3 L}\right]^2} \quad \text{with} \quad \frac{\mu}{R_0^2} = 60\ \text{GV}$$

- Space instruments.

PAMELA : small acceptance but polar orbit $\Rightarrow$ 10^{-7} level on anti-^{4}He

AMS : large acceptance $\Omega ST = 1.8\times10^4\ m^2\ sr\ s$ but mostly equatorial $\Rightarrow$ 200 antiprotons during the shuttle flight of 1998 $\Rightarrow$ 10^{-9} level on anti-nuclei during the space station stage with $\Omega ST = 2\times10^7\ m^2\ sr\ s$

Cosmic Ray Neutron Monitors, 1997

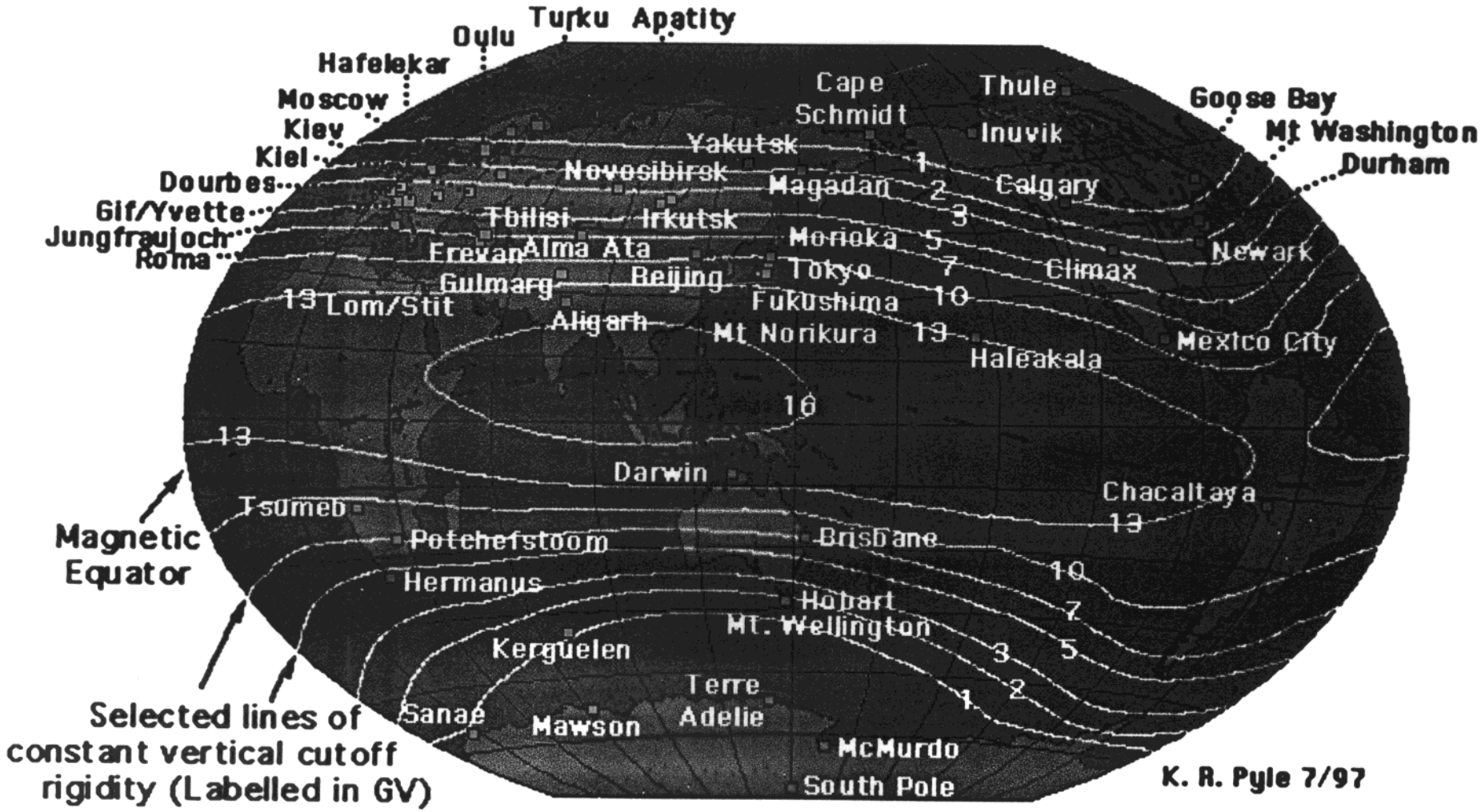

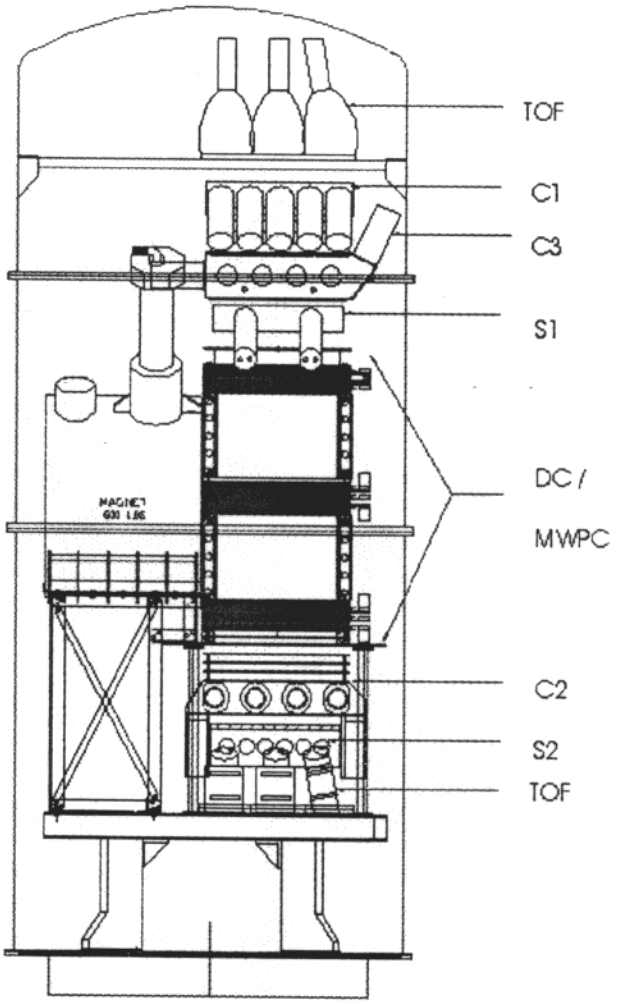

Balloon-borne IMAX

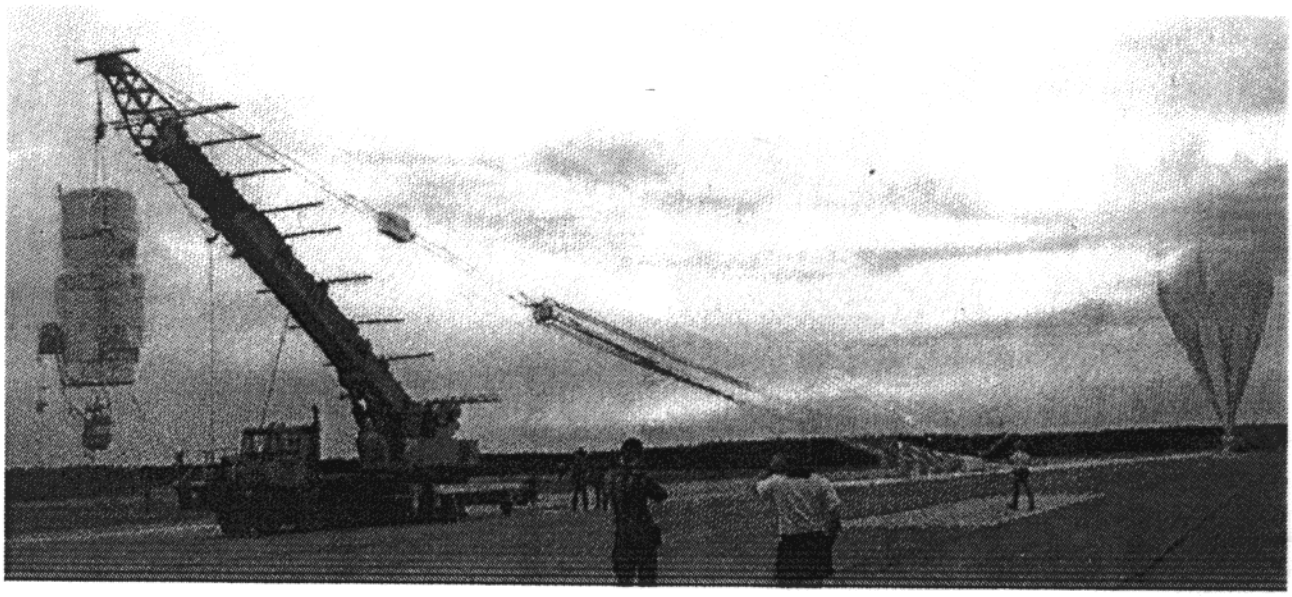

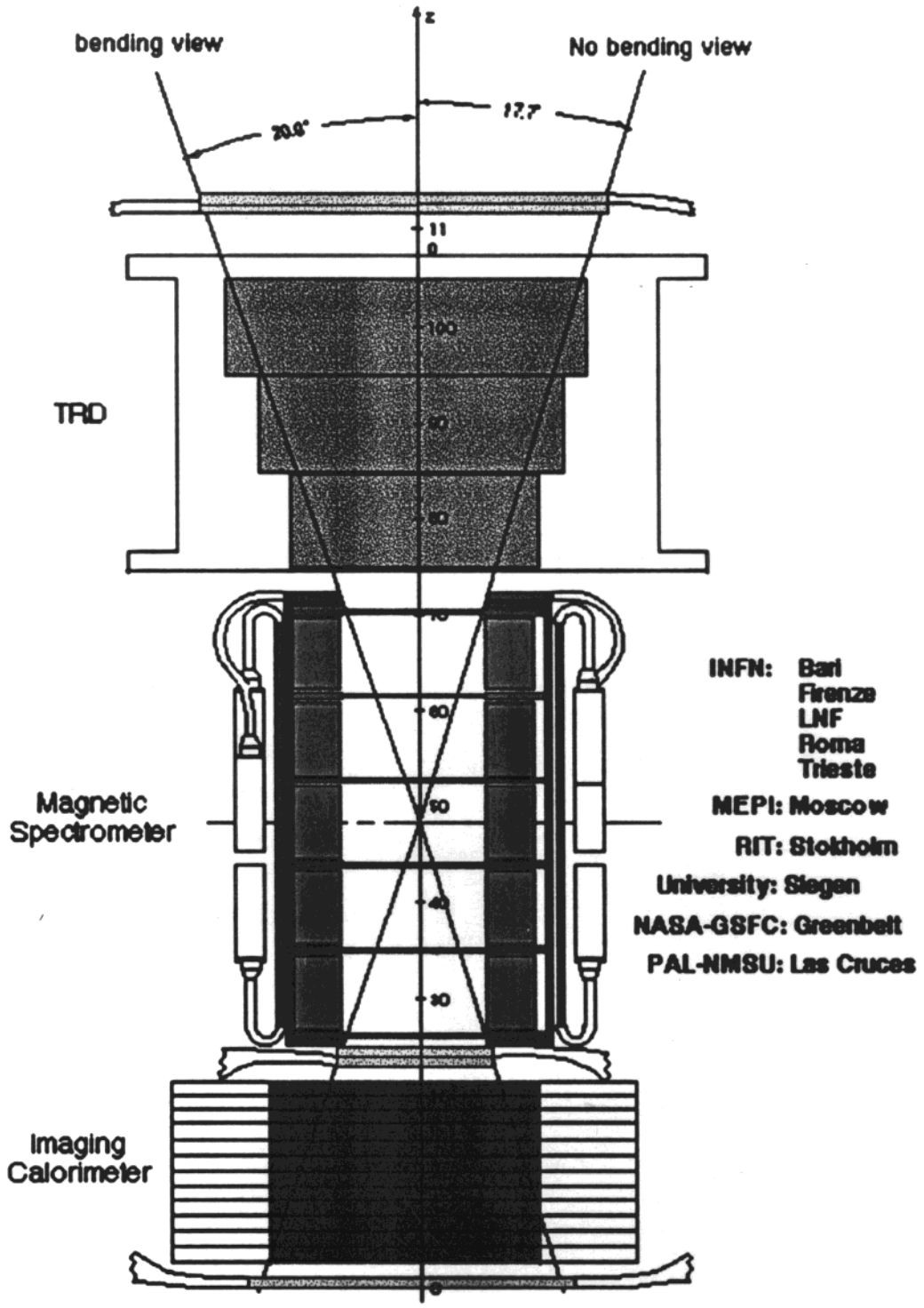
bending view
No bending view
20.8°
17.7°
z
11
0
100
TRD
80
50
10
60
Magnetic
Spectrometer
90
40
30
Imaging
Calorimeter
INFN: Bari
Firenze
LNF
Roma
Trieste
MEPI: Moscow
RIT: Stokholm
University: Siegen
NASA-GSFC: Greenbelt
PAL-NMSU: Las Cruces

PAMELA

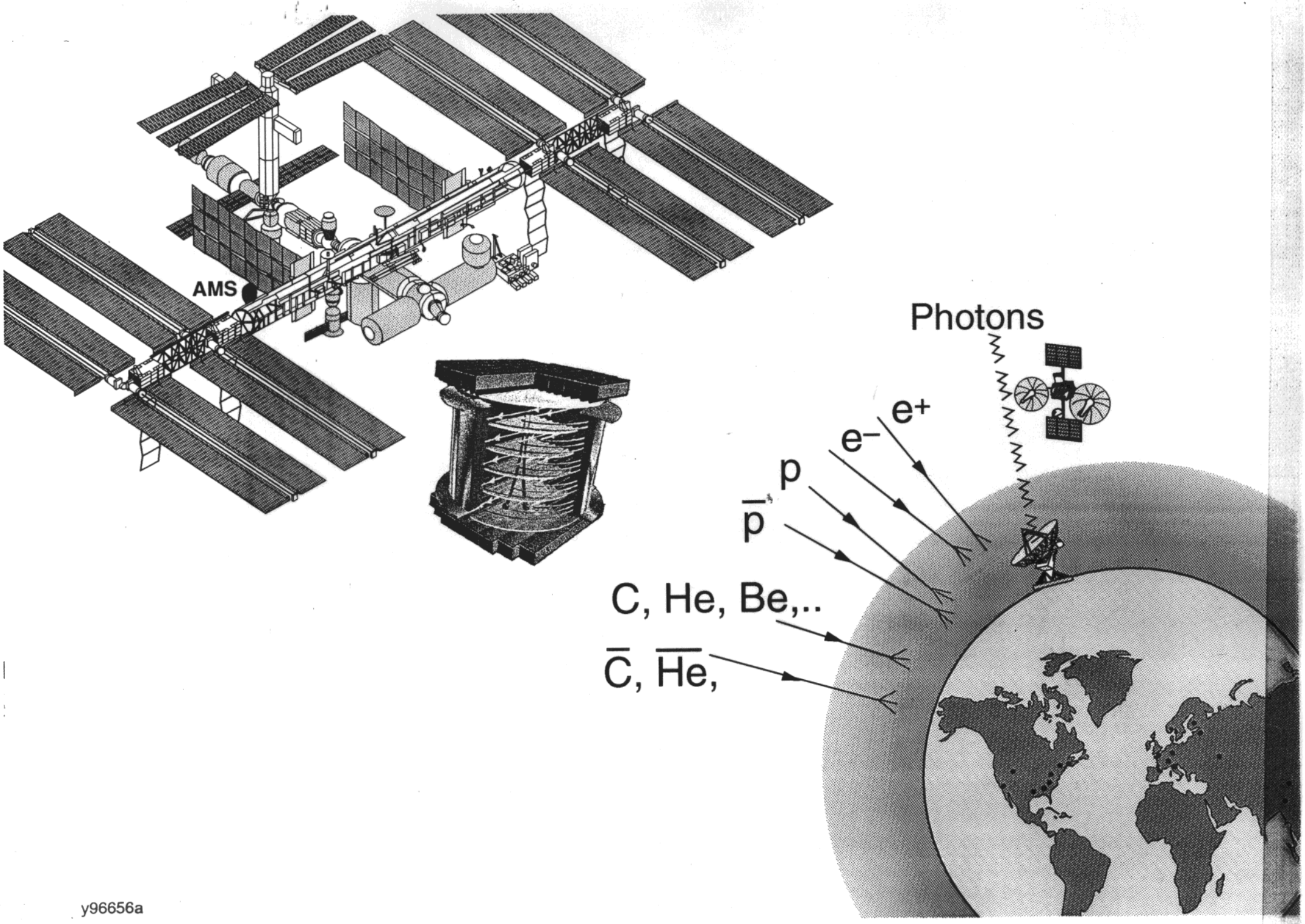
AMS
Photons
e+
e−
p
p̄
C, He, Be,..
C̄, He,
y96656a

Geomagnetic cut-off & AMS acceptance included.

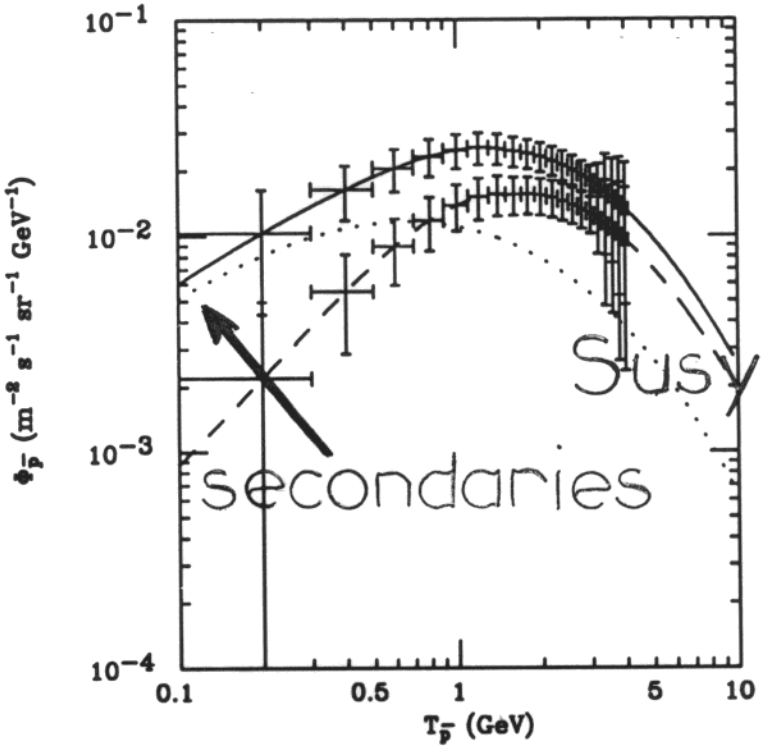

Figure 18

Figure 3: Expected distribution of measurements with the AMS Shuttle flight. The lower sequence of crosses corresponds to secondary antiprotons alone while the upper sequence includes a significant contribution of primary antiprotons from neutralino annihilations.

IS proton flux $\rightarrow$ 25% uncertainty on $\Phi_{\bar{p}}$.

Uncertainty on the diffusion coefficient K
$\rightarrow$ $\Delta\Phi_{\bar{p}}/\Phi_{\bar{p}} = 45$ % at 100 MeV and 20% at 600 MeV.

Antideuterium detectability

On board AMS during the space station phase

- Between 100 MeV & 3 GeV : SUSY antideutons.

  $\Omega STE = 1.6\times10^{7}$ m^2 sr s GeV solar minimum

  $\Omega STE = 9.8\times10^{6}$ m^2 sr s GeV solar maximum

  $\Phi_{\overline{D}} = 10^{-6}$ m^{-2} sr^{-1} s^{-1} GeV^{-1} $\Rightarrow$ 10 $\overline{D}$

- Between 3 GeV & 10 GeV : secondary antideutons.

  $\Omega STE = 1.3\times10^{8}$ m^2 sr s GeV solar minimum

  $\Omega STE = 1.1\times10^{8}$ m^2 sr s GeV solar maximum

  $\Phi_{\overline{D}} = 10^{-8}$ m^{-2} sr^{-1} s^{-1} GeV^{-1} $\Rightarrow$ 1 to 2 $\overline{D}$

On board BESS

$\Omega STE = 1\text{-}2\times10^{4}$ m^2 sr s GeV

Should run for a long time !

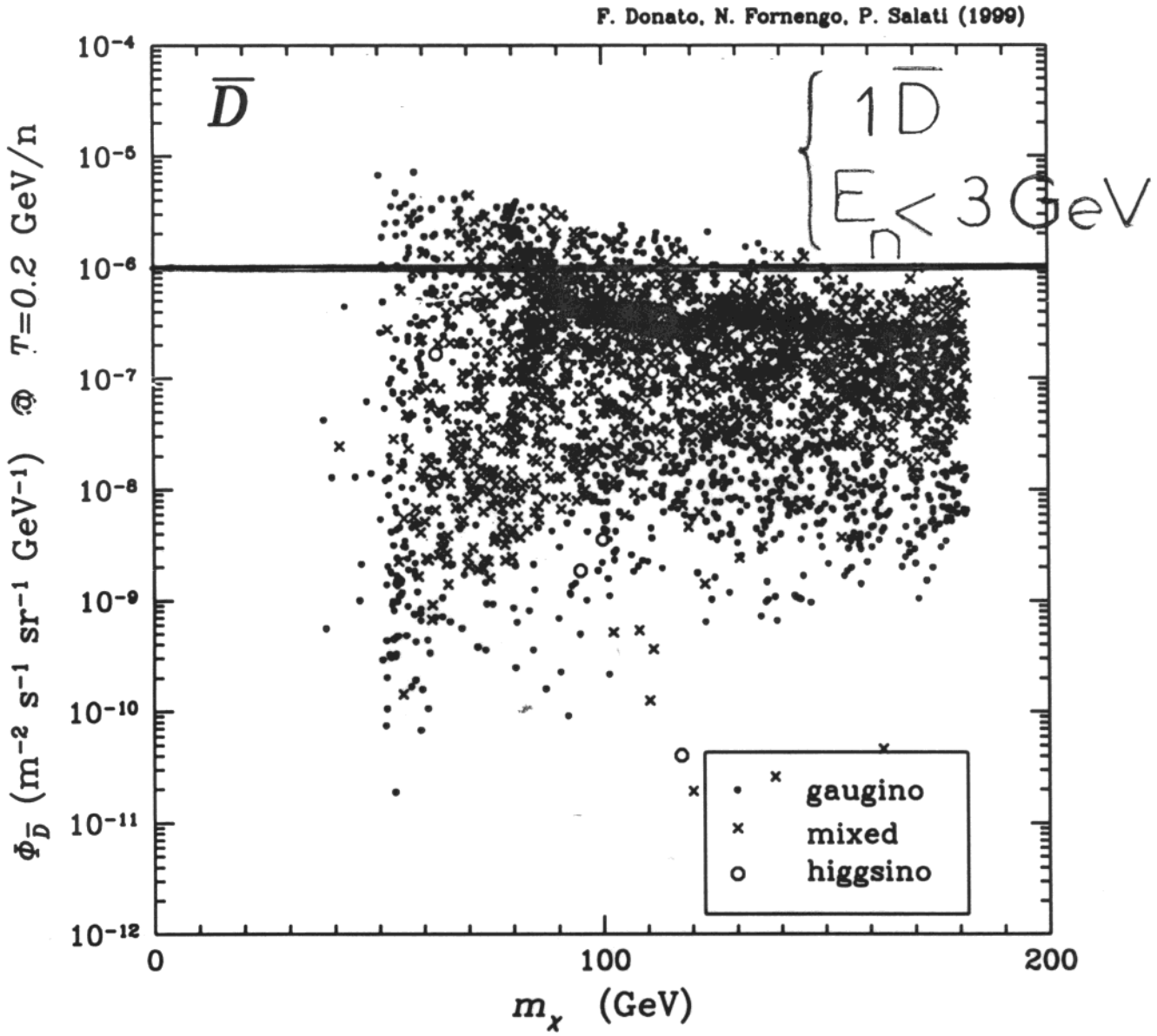
F. Donato, N. Fornengo, P. Salati (1999)
$\overline{D}$
1 $\overline{D}$
$E_n < 3$ GeV
$\Phi_{\overline{D}}$ (m^{-2} s^{-1} sr^{-1} GeV^{-1}) @ T=0.2 GeV/n
m_χ (GeV)
gaugino
mixed
higgsino
10^{-4}
10^{-5}
10^{-6}
10^{-7}
10^{-8}
10^{-9}
10^{-10}
10^{-11}
10^{-12}
0
100
200

A word of caution !

- Better determination of the proton flux needed between 5 and 20 GeV.

- Consistent determination of the diffusion coefficient K from B/C measurements.

- Solar modulation $\phi_{\bar{p}}^{TOA}$ vs $\phi_{\bar{p}}^{IS}$

- Antiproton energy losses
  Ionisation
  Elastic scattering on IS nuclei

- Diffusive reacceleration
  Heinbach & Simon ApJ 441 (1995) 209

- Nucleus-nucleus interactions
  Simon, Molnar & Roesler ≠ Gaisser & Schaefer

However !

The larger the secondary antiproton flux at low energy, the more constrained is SUSY by the BESS and AMS data.

Proton flux poorly determined at high energy.

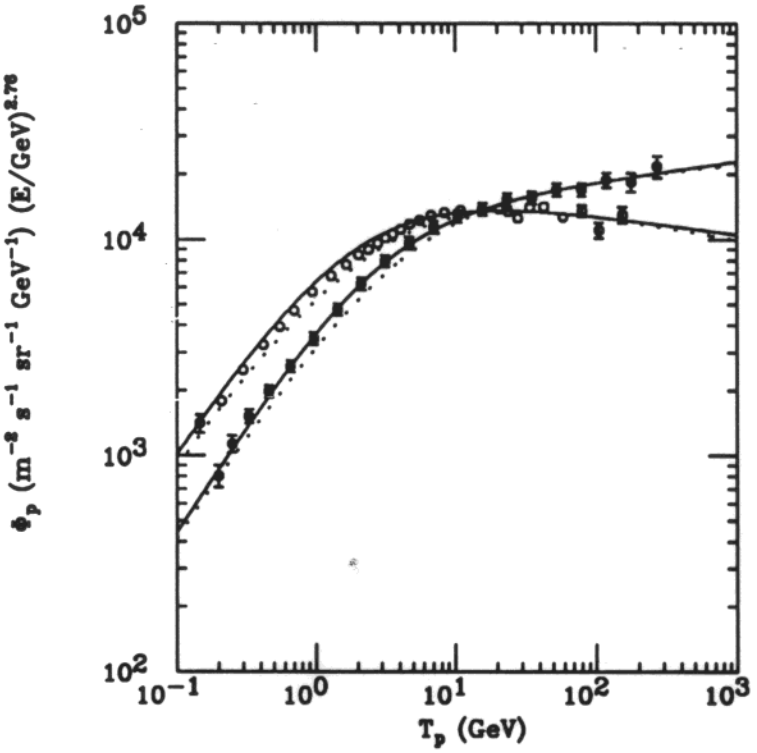

Figure 2

Figure 4: TOA spectra of IMAX (full circles) and of CAPRICE (open circles) with our best–fit curves with parametrization as a function of the energy (solid lines) and the rigidity (dotted lines).

$$\Phi_{\mathrm{p}}^{\mathrm{IS}} = A\,\beta\,E^{-\gamma}$$

$$A = (1.595 \pm 0.365)\ \text{protons}\,\text{cm}^{-2}\,\text{s}^{-1}\,\text{sr}^{-1}\,\text{GeV}^{-1}$$

$$\gamma = 2.76 + 0.13 - 0.15$$

The B/C Ratio and the Diffusion Coefficient K

- $\mathcal{R} \geq \mathcal{R}_0 : K = K_0 \mathcal{R}^{0.6}$
- $\mathcal{R} \leq \mathcal{R}_0 : K = K_0 \mathcal{R}_0^{0.6-\delta} \mathcal{R}^{\delta}$

D. Maurin (LAPTH) : preliminary

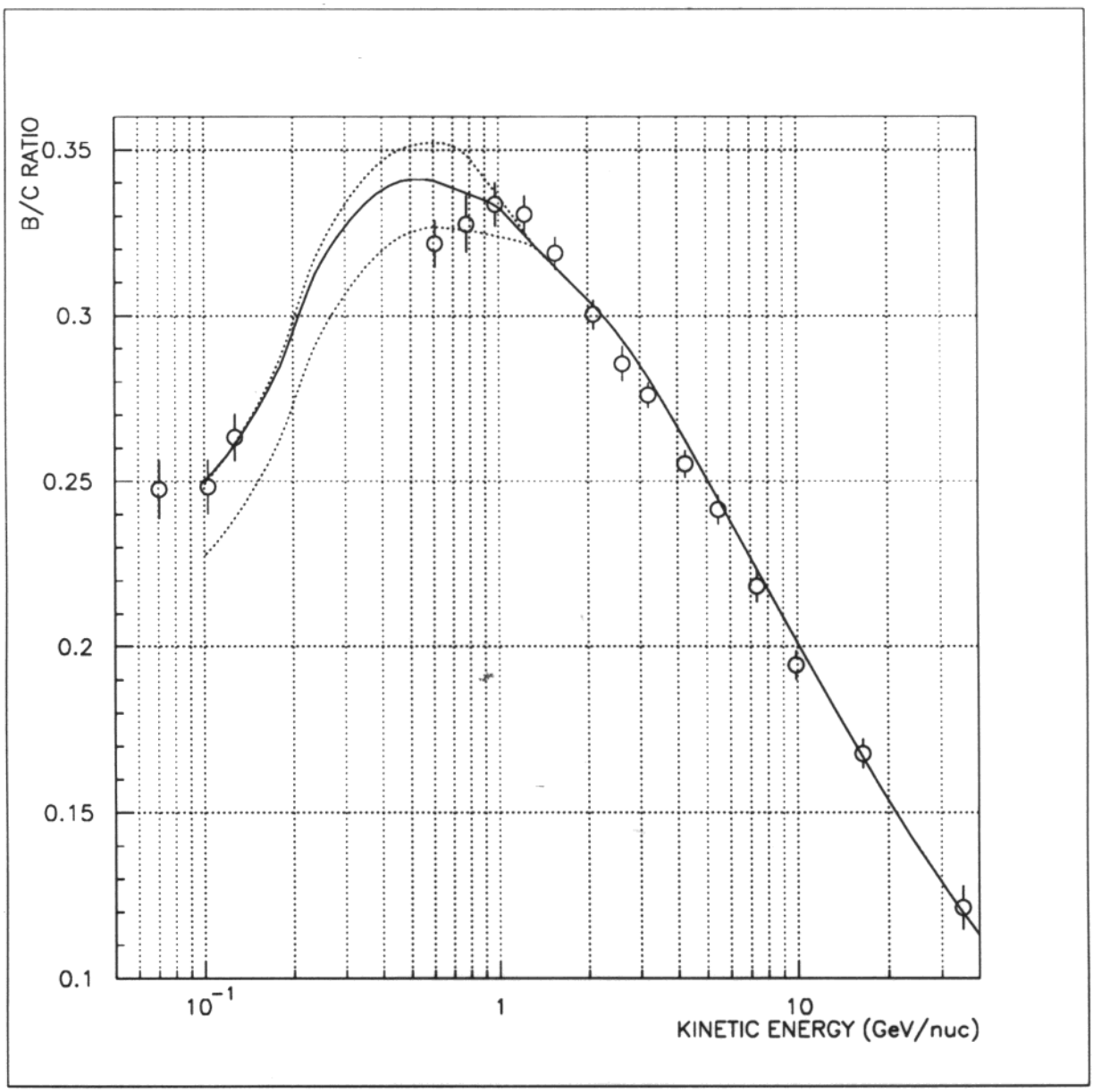

Figure 8: The B/C ratio as a function of the kinetic energy per nucleon. Ionization losses and reacceleration have not been included. The isotopes ^{10}B and ^{11}B are produced from the spallation of the CNO elements. Cross sections are borrowed from Read & Viola (1984) while the CNO abundances are from Duvernois *et al.* (1996). The solid curve corresponds to $\delta = 0.08$ and $\mathcal{R}_0 = 3.8$ GV whereas, for the dashed curves, $\delta = 0$ and $\mathcal{R}_0 = 3.2$ Gv (max) and 4.2 GV (min).

Solar Modulation : Force Field Approximation.

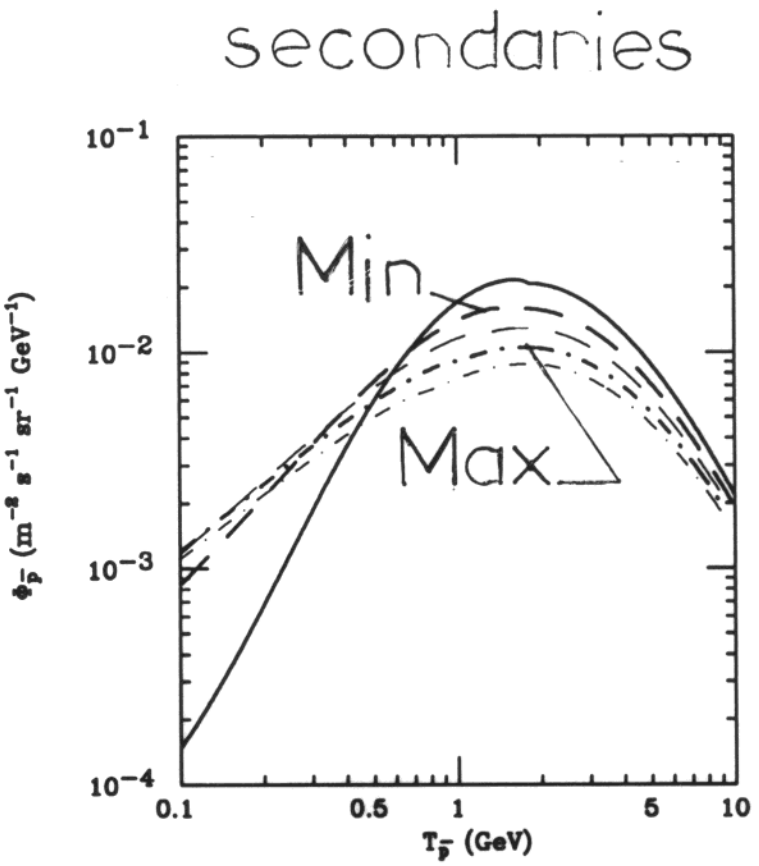

Figure 8

Figure 5: Solar modulation of the IS median secondary antiproton flux (solid line). Thick dashed (thick dot–dashed) line is the solar–modulated spectrum at minima (maxima) when the modulation parameter Δ is obtained from a parametrization of the primary proton spectrum as a function of energy. The light curves refer to a parametrization as a function of rigidity.

$$E_{\rm n}^{\rm TOA} = E_{\rm n}^{\rm IS} - \frac{Z}{A}\Delta \quad \text{and} \quad \Phi^{\rm TOA}/\Phi^{\rm IS} = \left(p_{\rm n}^{\rm TOA}/p_{\rm n}^{\rm IS}\right)^2$$

for a rigidity $\leq$ 200 MV and with 0.32 GV $\leq \Delta \leq$ 0.8 GV

Solar Modulation
Effect on Primary Susy Antiprotons

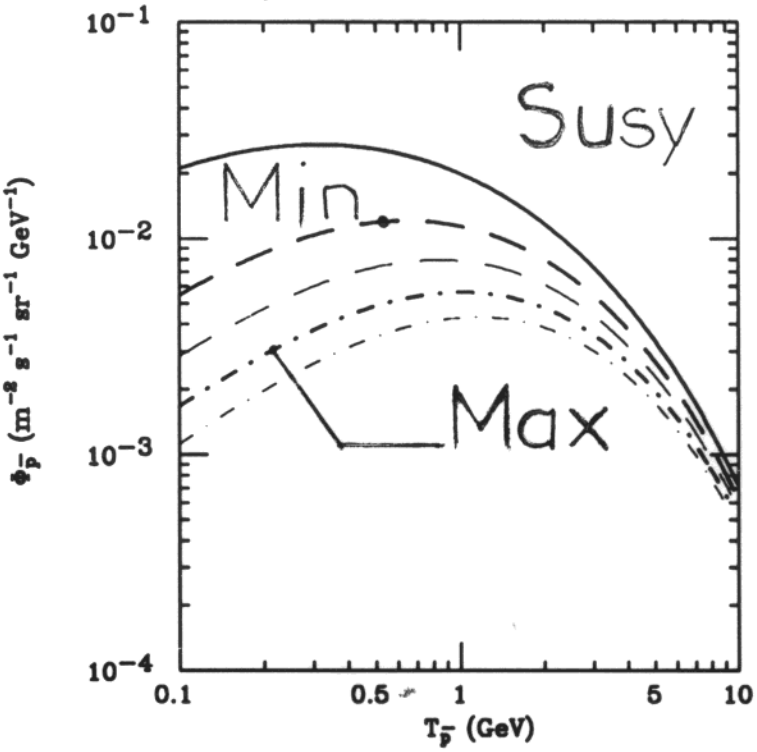

Figure 9

Figure 6: Solar modulation of the IS antiproton flux, due to neutralino annihilation for the representative neutralino configuration with $m_\chi = 62$ GeV, $P = 0.98$ and $\Omega_\chi h^2 = 0.11$. Solid line is the IS spectrum. Thick dashed (thick dot–dashed) line is the solar–modulated spectrum at minima (maxima) when the modulation parameter Δ is obtained from a parametrization of the primary proton spectrum as a function of energy. The light curves correspond to a parametrization as a function of rigidity.

Energy losses

- Ionisation losses
- Elastic scattering on Interstellar H

inelastic_no annihilation.

$\bar{p}$ loses $T_{\bar{p}}/2$

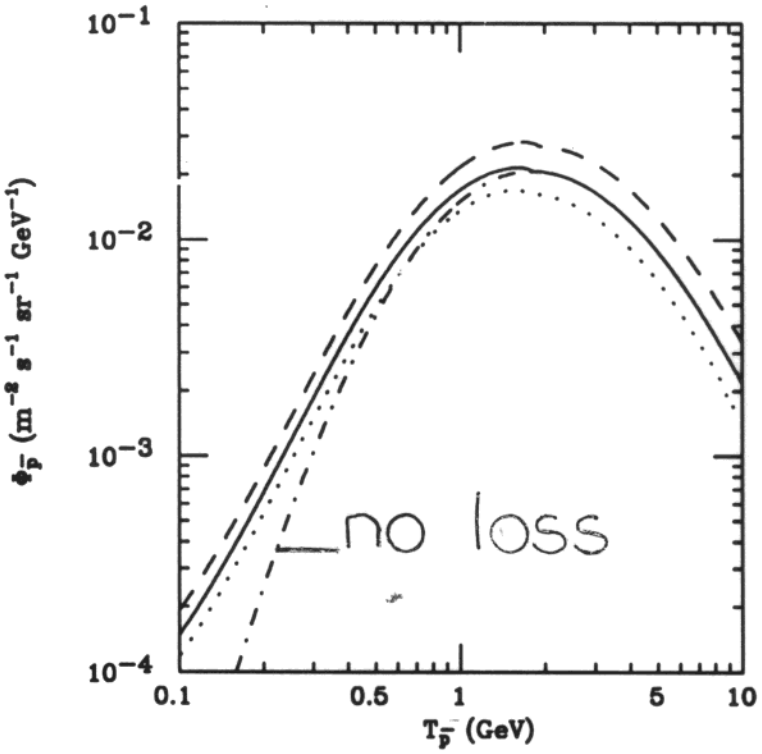

$$\frac{dn}{dt} = -\frac{d\,bn}{dE}$$

Figure 5

$$b = \dot{E} = -\frac{T_{\bar{p}}}{2}\sigma n_H v_{\bar{p}}$$

Figure 7: IS secondary antiproton spectra as a function of the $\bar{p}$ kinetic energy. Solid, dotted and dashed lines denote the fluxes obtained from the median, minimal and maximal IS primary proton fluxes. The dot–dashed line denotes the median $\bar{p}$ spectrum, when the $\bar{p}$ energy losses are neglected.

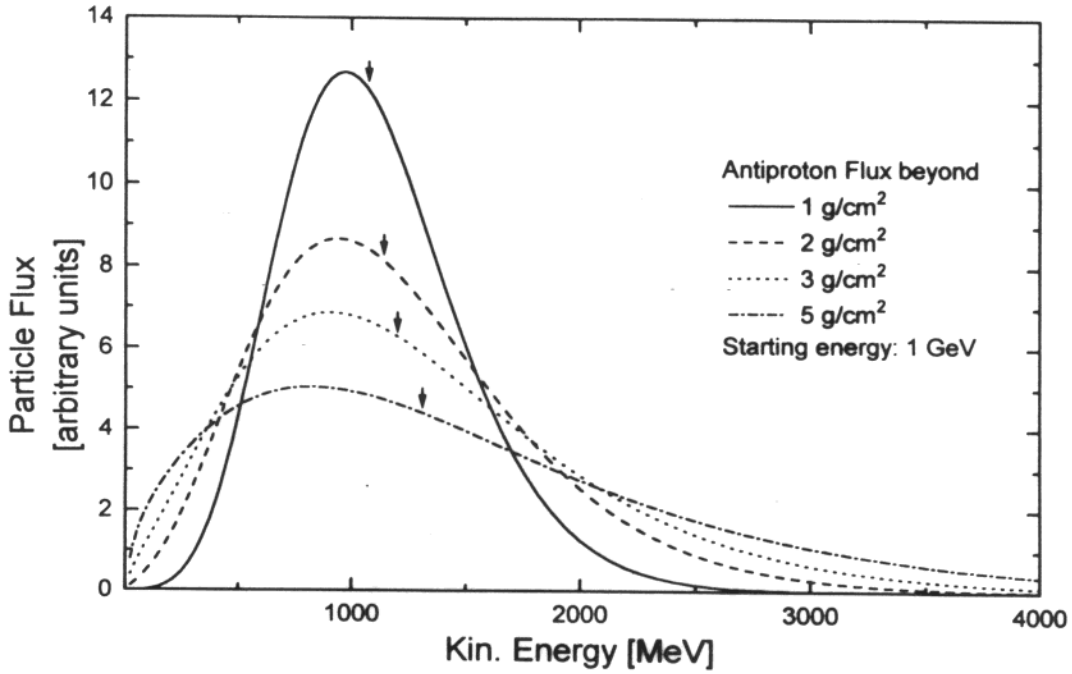
Particle Flux
[arbitrary units]
Kin. Energy [MeV]
Antiproton Flux beyond
1 g/cm²
2 g/cm²
3 g/cm²
5 g/cm²
Starting energy: 1 GeV

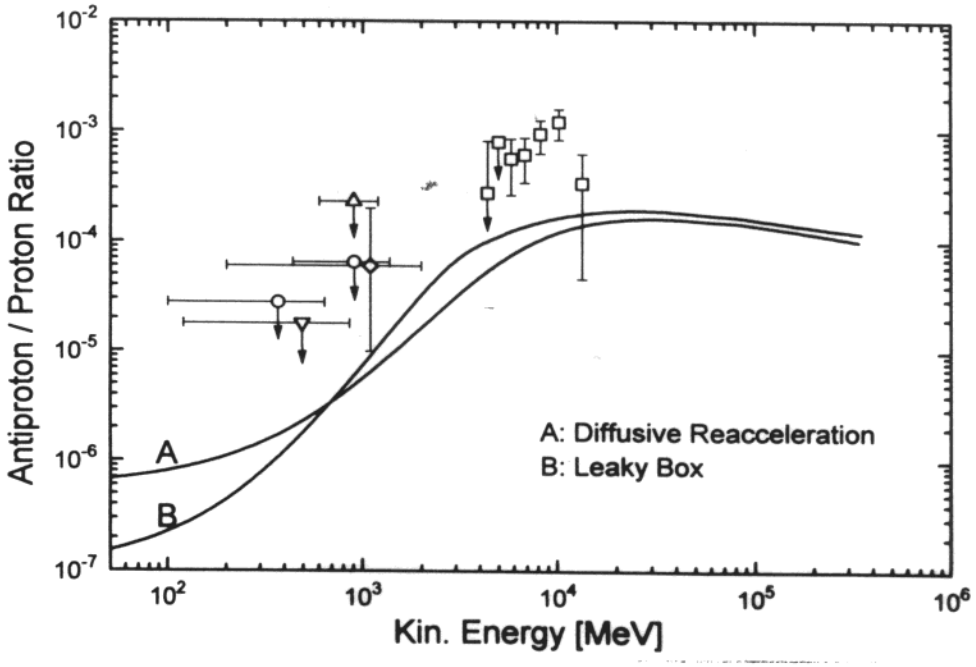
Antiproton / Proton Ratio
Kin. Energy [MeV]
A: Diffusive Reacceleration
B: Leaky Box
A
B

Conclusions

1. $\bar{p}$ data & Secondary source OK

2. Data precision : Susy sensitive

3. However, large systematic uncertainties for secondary $\bar{p}$

   Hope!

4. $\bar{D}$: smoking gun

   Clear signal _ Low flux